Deep-Sea Research II 58 (2011) 1768–1780

Contents lists available at ScienceDirect

Deep-Sea Research II

journal homepage: www.elsevier.com/locate/dsr2

Transport of the North Atlantic Deep Western Boundary Current about 39°N, 70°W: 2004–2008

J.M. Toole *, R.G. Curry, T.M. Joyce, M. McCartney, B. Peña-Molino

Woods Hole Oceanographic Institution, 266 Woods Hole Road, MS# 21, Woods Hole, MA 02543, USA

ARTICLE INFO

Article history:
Received 12 October 2010
Accepted 12 October 2010
Available online 27 January 2011

Keywords:
Deep currents
Mooring systems
North Atlantic Ocean
Deep Western Boundary Current
Gulf Stream
Transport

ABSTRACT

Begun in spring 2004, a sustained measurement program – Line W – is returning high-resolution observations of the North Atlantic's Deep Western Boundary Current (DWBC) southeast of New England. The study focuses on the cold limb of the Atlantic Meridional Overturning Circulation near the boundary between the subpolar and subtropical gyres. The field study consists of a 6-element, continental-slope-spanning moored array on a line underlying an altimeter satellite ground track, and periodic reoccupations of a full-depth hydrographic section along the line extending from the continental shelf towards Bermuda. Here, data from the first 4 years of the array (May 10, 2004–April 9, 2008) are analyzed along with 9 realizations of the section. The array, a mix of Moored Profiler and discrete, fixed-depth instrument moorings, returned temperature, salinity and horizontal velocity data with various temporal and depth resolutions. After averaging to filter inertial, tidal and other high-frequency motions, the combined moored data set was binned to the lowest common temporal resolution of 5-days (the nominal burst sample interval of the Moored Profilers) and interpolated to 2-dbar vertical resolution. Temperature, salinity, dissolved oxygen, tracer chemical concentrations and direct velocity data were acquired on the hydrographic cruises. The present work focuses on the 4-year-mean and time-varying meridional transport in 4 layers bounded by neutral density surfaces: Upper and Classical Labrador Sea Waters, Iceland-Scotland Overflow Waters and Denmark Strait Overflow Waters. The 5-d, 4-layer-summed meridional transport estimates range between −3.5 and −79.9 Sv with a record mean average transport of −25.1 Sv and standard deviation of 12.5 Sv. Bias adjustment to account for the finite width of the moored array increases the 4-layer mean transport estimate to −28.7 Sv. At time scales longer than about 1 month, the variations in equatorward DWBC transport appear correlated with meridional position of the Gulf Stream North Wall with stronger transport observed when the Stream is displaced south.

1. Introduction

The Meridional Overturning Circulation (MOC) of the North Atlantic Ocean at mid-latitude involves poleward net transport of warm water by the Gulf Stream and southward net flow of colder intermediate and deep waters within a Deep Western Boundary Current (DWBC) (Stommel, 1965). Both current systems are partially compensated by local recirculations (Hogg, 1992) as well as by interior flows (Bower et al., 2009). Comprehension of how these major limbs of the global current system and their associated regional recirculations vary on decadal time scale is incomplete. In particular, we lack understanding of how interannual variations in air–sea exchange and water mass modification at high latitudes are transmitted equatorward, and what impacts or feedbacks such signals may have for the Atlantic-wide circulation, the surface temperature distribution and air–sea exchange. Limiting advance in understanding is the lack of long, well-resolved records to document interannual signals in water properties, stratification, and transport of the North Atlantic's MOC system elements. Here, estimates of DWBC transport based on the initial 4 years of data from a sustained measurement program southeast of New England are presented. The program, named Line W in memory of L. Valentine Worthington (a physical oceanographer at the Woods Hole Oceanographic Institution who devoted a considerable part of his career to measuring and understanding the water properties and flows in and about the Gulf Stream/DWBC system), consists of a moored array spanning the continental slope about 39°N, 70°W and a program of repeated ship-based hydrographic/direct-velocity sections along the array and extending into the Sargasso Sea (Fig. 1). Following some background discussion, Section 2 details the observational program, data processing procedures and

* Corresponding author.
E-mail address: jtoole@whoi.edu (J.M. Toole).
URL: http://www.whoi.edu/people/jtoole (J.M. Toole).

0967-0645/$ - see front matter © 2011 Elsevier Ltd. All rights reserved.
doi:10.1016/j.dsr2.2010.10.058

analysis methods. Results are presented in Section 3 and discussed in Section 4.

The past four decades constituted a most unusual chapter in North Atlantic climatic history, characterized by an extreme fluctuation in large-scale atmospheric circulation and precipitation patterns. A significant fraction of that variability is associated with the North Atlantic Oscillation (NAO), a phenomenon that collectively involves changes in the strength and geography of atmospheric mass (e.g., Hurrell and van Loon, 1997), wintertime storm activity (Rogers, 1990), and related air–sea exchanges of heat (Cayan, 1992a, b), fresh water (Hurrell, 1996) and momentum (Visbeck et al., 1998). The ocean responded in an equally conspicuous manner including prominent shifts in the patterns of SST anomalies (Deser and Blackmon, 1993; Kushnir, 1994), convective activity (Dickson et al., 1996), water mass properties (Lazier, 1995; Talley, 1996; Dickson et al., 2002), intensity of gyre circulations (Greatbatch et al., 1991; Curry and McCartney, 2001; Häkkinen and Rhines, 2004) and efflux of sea ice and fresh water from the Arctic (Dickson et al., 2000). From the early 1960s to the mid-1990s, the NAO evolved from an extreme negative state to a prolonged and extreme positive phase. It remains an open question whether this signal reflects a global climate shift or has anthropogenic causes. But regardless of cause, the entire water column of the Labrador Sea changed radically in this time frame. In the latter part of the 1990s, the extreme high NAO phase abruptly ended, production of LSW slackened considerably, and these sustained cooling and freshening trends were halted or partly reversed. However, the deeper water masses that originate in the Nordic Seas continued to freshen. Dickson et al. (2002) showed that both the Denmark Strait Overflow Water (DSOW) and Iceland-Scotland Overflow Waters (ISOW) decreased in salinity at a sustained rate of approximately 0.01 per decade, due in part to a long-term freshening of the upper 1–1.5 km in the Nordic Seas (Curry and Mauritzen, 2005). The emerging picture suggests that the system by which the entire intermediate to deep North Atlantic is ventilated – convection, overflows, and entrainment – has changed over the past four decades. These changes have already led to sustained, widespread, and surprisingly rapid property shifts in the headwaters of the Atlantic overturning circulation. The ocean signatures of these changes are now spreading into the lower latitudes and modifying the intermediate and deep water mass characteristics and stratification there. (These signals at Line W will be reported elsewhere.) How is the circulation responding to these changes?

Several theoretical/modeling frameworks are now available that provide insight. One particularly intriguing mechanism was explored by Spall (1996) for the classic double-gyre wind forcing of a layered primitive ocean model. A decadal fluctuation in the depth and zonal penetration of the Gulf Stream and its recirculations was induced when a fixed strength DWBC was supplied from the north with a fixed potential vorticity anomaly (lower relative to the background). The variability mechanism involved the impact of the low potential vorticity (PV) waters entrained (or not) at the point where the DWBC crosses under the Stream on the GS instabilities, and thus on the downstream growth of the current. The feedback loop was closed by the dependence of that entrainment on the GS strength. While this is an internal variability mechanism (because the specified DWBC transport and PV were constant), we can imagine an externally forced analog since we know the PV of the DWBC has pronounced interannual/decadal variability. Joyce et al. (2000) examined this further by imposing a time-variable DWBC transport and diagnosing the response of the Gulf Stream to this variability; this was in the context of a self-sustained oscillator model examining links between the NAO, Gulf Stream position, and DWBC transport. Models of the dynamical response of the Gulf Stream to time-dependent, high latitude PV signals (Yang and Joyce, 2003) suggest a different blocking effectiveness for LSW water vs. overflow water anomalies, with the former more likely to be diverted at the crossover than the latter. It is also likely that there are internal modes of variability in the strong recirculation regimes of mid-latitude basins. A series of papers by Berloff and colleagues (Berloff and Meacham, 1998a, b; Berloff and McWilliams, 1999a, b) explores the rather chaotic low frequency behavior of strongly inertial systems. Assessing the modes of variability of the real ocean has been difficult because high resolution models continue to have difficulty accurately reproducing the structure of the Gulf Stream and DWBC system.

Although previous studies have provided us with a basic dynamical and kinematic framework to qualitatively anticipate how the climate system might be operating, we still lack the data – sufficiently well-sampled in space and time – to formally test those concepts. Therefore, in 2004 we initiated an observational system in the DWBC southeast of New England designed to quantify the properties, structure, and transport of the waters of the Northwest Atlantic DWBC. The system utilizes a variety of moored instruments and coordinated shipboard measurements with the resulting data – in combination with other ocean observing system components – supporting detailed investigations into the DWBC and Gulf Stream at mid-latitude. Here we focus on time-average DWBC transport and its variability in a 4-year period 2004–2008; a study of water mass variability from a chemical tracer standpoint on Line W being led by Dr. William Smethie, Jr. at the Lamont Doherty Earth Observatory will be reported elsewhere. Companion papers documenting co-variability of DWBC water properties and transport are in preparation.

Section 2 below documents the observations and data reduction and analysis procedures. Those readers not interested in the details of the field program and data processing are invited to skip to the description of the transport estimation procedures in Section 2.4. Results are presented in Section 3 and discussed in Section 4.

2. Observations and methods

2.1. Measurements

The Line W field program consists of two main elements: repeated shipboard sampling of the water properties and velocity field along an altimeter-satellite ground track that is roughly orthogonal to the continental slope isobaths, and maintenance of a 5-element moored array on that same line spanning the slope between the 2200 and 4100 m isobaths (Fig. 1, Table 1). (For part of the present analysis period, a 6th mooring was deployed at the 4700 m isobath.) The Slope Water southeast of New England is bounded by a front at the shelf break and by the North Wall of the Gulf Stream, a region Csanady and Hamilton (1988) termed the Slope Sea. Based on an along-track coordinate system with origin on the shelf at $40^{\circ}17'$N, $70^{\circ}12'$W (86 m depth), the shelf break (200 m isobath) lies at distance 48 km and the 2200 m isobath at distance 87 km. Mooring #5 was situated at distance 279 km, which is also the mean position of the SST front marking the Gulf Stream North Wall based on US Navy frontal analysis maps for the January 2004–October 2008 period.

During the first 4 years of the Line W program (May 2004–2008), cruises were run twice per year, typically in spring and fall with mooring deployment/recovery work on the spring trips and shipboard sampling on both (Table 2). A standard set of stations were targeted for occupation on each cruise (Fig. 1). The latitudinal extent of the station work was dictated by the available ship time, weather conditions and the fact that the mooring work on the spring cruises had highest priority. The Slope Waters (shelf break to North Wall) were fully sampled on every cruise, but the station sites south of the Gulf Stream were occupied only intermittently. Continuous temperature, salinity and dissolved oxygen profile data were acquired at each station along with discrete water samples that were analyzed for salinity, dissolved oxygen, and transient tracer concentrations. Direct velocity observations were acquired continuously on the cruises with standard hull-mounted acoustic Doppler current profilers (upper ocean) and at each station using Lowered ADCP instrument systems (full-depth velocity data). Joyce et al. (2005) described the subset of Line W ship data that were available at the time and made comparisons to previously collected data on this line.

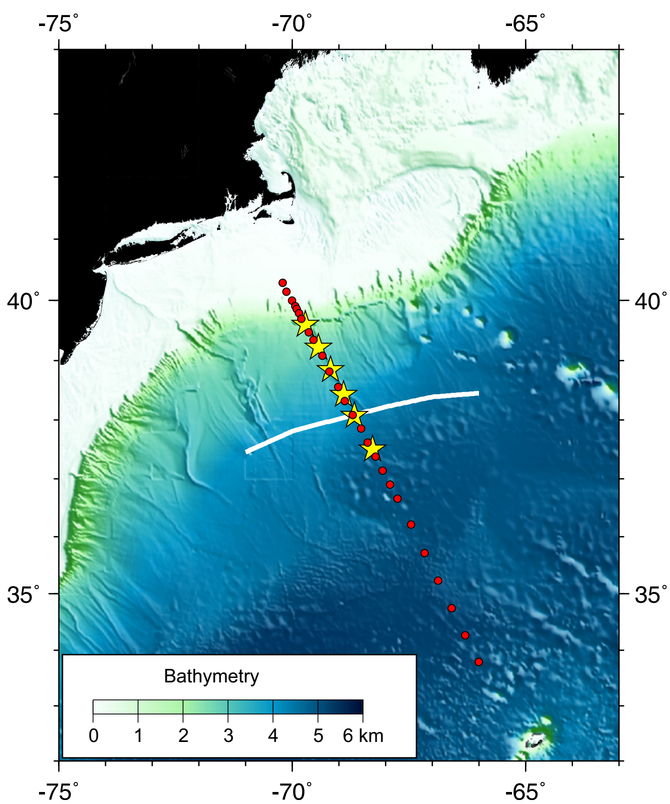

Fig. 1. Location of the Line W moorings (stars) and regularly sampled ship stations (dots) superimposed on the regional bathymetry. The color scale ranges from white (less than 200 m water depth) to dark blue (more than 5000 m depth). The white line segment marks the mean position of the Gulf Stream North Wall based on US Navy frontal analysis data.

The moored array consisted of a mix of fixed-depth and profiling sensor systems. The mix was a trade-off between the high vertical resolution data possible from moored profiler instruments and the excellent temporal resolution characteristic of fixed-depth sensors. The combination of instruments also ameliorated some of the risk of profiling instrumentation in which a single instrument failure can have huge impact. Mooring nos. 1, 3 and 5 were equipped with McLane Moored Profiler (MMP) instruments (one per mooring) along with Vector Averaging Current Meters (VACMs) and Sea Bird Electronics temperature/conductivity (T/C) sensors above and below each profiled depth segment. (Not all deployments of Moorings 1 and 3 had top VACMs.) Moorings 2 and 4 supported vertical distributions of VACMs and T/C sensors. (Mooring 6 was fitted just with VACMs.) The depths of the shallowest sensors on most of the moorings were monitored with pressure sensors integrated into either VACMs or T/C sensors. Depth time series for the other instruments on the moorings not so equipped were derived using a simple mooring response model. The present study considers moored array data from the time period 10 May 2004 to 9 April 2008.

Profiling endurance of the MMPs necessitated annual servicing of those moorings; the current meter moorings were recovered and redeployed at 2-year intervals. Moorings 1 and 3 typically extended up to within 100 m of the surface. Anticipating that strong surface-intensified currents at site 5 could negatively impact the ability of the MMP to profile, the top of this mooring was set at ~1000 m depth. Program focus on intermediate and deep waters motivated the capping of Moorings 2 and 4 at 1000 m depth also. The shallowest current meter on Mooring 6 was at approximately 400 m depth. The MMPs were typically programmed to burst sample a set of 4 one-way profiles every 5th day of the deployments. (The 2005–2006 settings of Moorings 3 and 5 were programmed with a 7.5-d burst interval, while the 2007–2008 MMP at Mooring 1 returned 6 one-way profiles per burst with 6-h between profiles.) Within each burst, profiles were typically initiated approximately every 9.5 h to exploit a fortuitous characteristic of the Line W array latitude. This time interval

Table 1
The Line W moored array. Observations from these sites between 10 May 2004 and 9 April 2008 are analyzed here. The instrument depths reported are averages over the 4 years of the array; the MMP depth ranges are approximate. MMP: McLane Moored Profiler, VACM: Vector Averaging Current meter.

	Latitude	Longitude	Bottom depth (m)	Instrumentation and mean depths
1	39°36.0′N	69°43.1′W	2242	MMP: ~60 m to 2145 m[a] T/C sensors: 62, 2126 m VACMs: 55[a], 2126 m
2	39°13.0′N	69°26.7′W	2752	T/C sensors: 1031, 1331, 1631, 1927, 2224, 2318, 2411, 2536, 2646, 2677 m VACMs: 1031, 1631, 2224, 2677 m
3	38°50.6′N	69°11.1′W	3248	MMP: ~60 to 3150 m T/C sensors: 121, 3203 m VACMs: 50,[a] 3203 m
4	38°25.5′N	68°54.0′W	3686	T/C sensors: 1043, 1343, 1644, 1943, 2241, 2688, 2927, 3138, 3234, 3316, 3397, 3433, 3607 m VACMs: 1043, 1644, 2241, 2688, 3234, 3575[a] m
5	38°4.4′N	68°40.0′W	4110	MMP: ~1000 to 4050 m T/C sensors: 1007, 4079 m VACMs: 1007, 4079 m
6	37°30.0′N	68°16.8′W	4701	VACMs[a]: 484, 784, 1084, 1584, 2084, 2584, 3084, 4084 m

[a] Not full records for entire 4 years.

Table 2
Line W cruises 2004–2008. Bad weather prevented recovery of all of the moorings on cruise OC446; the remaining moorings were recovered on cruise EN454.

Cruise no.	Dates	No. of Stations	Activities
Oc401	4/28–5/6, 2004	18	Hydrography+Moorings 1–5
Kz1204	9/4–9/12, 2004	24	Hydrography
Oc411	4/25–5/4, 2005	22	Hydrography+Moorings 1, 3, 5, 6
Oc417	10/12–10/18, 2005	16	Hydrography
Oc421	4/5–4/15, 2006	17	Hydrography+Moorings 1–5
Oc432	10/19–10/26, 2006	21	Hydrography
Oc436	4/7–4/15, 2007	17	Hydrography+Moorings 1, 3, 5
En440	10/1–10/9, 2007	26	Hydrography
Oc446	5/10–5/20, 2008	17	Hydrography+Moorings 1 and 5 recovered
En454	9/18–9/24, 2008	–	Moorings 2, 3, 4 recovered

is roughly half the local inertial period and three quarters of the semi-diurnal tidal period. Thus the average of the 4 profiles in each burst has greatly reduced ageostrophic velocity and vertical displacement energy as compared to individual synoptic profiles. Moreover, these high-frequency signals may be extracted by linear combination of the profiles within each burst and studied separately (Silverthorne and Toole, 2008). The VACMs in the array returned velocity estimates averaged over 1/2 h time intervals while the T/C sensors recorded spot observations at 15 min increments.

Data return from the moored array was reasonable with two notable exceptions. Mooring 6, funded by the WHOI Ocean and Climate Change Institute as a complement to the main Line W array, suffered two major failures. The initial deployment of the mooring on 30 April, 2005 terminated prematurely on 11 May when a glass ball buoyancy element positioned just above the acoustic releases on the mooring imploded and caused the releases to open. The mooring was recovered and redeployed on 24 August. Then on 16 March 2006 during period of strong Gulf Stream flow, the main syntactic foam buoyancy sphere failed, causing the top of the mooring to sink to the bottom. Interestingly, the bottom-most 3 VACMs appear to have functioned after the mooring collapse, returning reasonable-looking velocity and temperature data until 2 October 2007 when the mooring was recovered. (Acceptable VACM performance may have been achieved because the distributed glass-ball buoyancy deployed above each VACM continued to hold these near-bottom current meters vertical after the mooring collapse.) We will use the deepest current measurements from Mooring 6 to characterize the magnitude of equatorward boundary-current deep-water transport that was missed by Moorings 1–5.

The other significant moored instrument failure was the MMP on the 2006–2007 setting of Mooring 1. After overcoming being stuck near the bottom of the mooring for the first 36 days of its deployment, this instrument profiled as programmed for 25 days but then abruptly stopped. No additional data were logged by the instrument and the MMP battery was totally drained on recovery. (The electronic watchdog subsystem in MMPs was subsequently enhanced to guard against this failure mode.) The fixed-depth sensors on this mooring functioned well throughout the deployment.

Shorter temporal gaps were observed in the other Moored Profiler records. The batteries in these vehicles would often be exhausted before the moorings were recovered and redeployed. Typically this introduced gaps of around 1 month in the MMP records. In addition, on an irregular basis, the MMPs failed to perform their scheduled full-depth profiles and were sometimes stuck for periods of a few days. Possibly due to drive wheel wear due to wire strumming in the strong Gulf Stream current, the MMPs on Mooring 5 experienced the most profiling difficulty and often failed to sample down to the bottom stop on the mooring. However, the fixed-depth sensors on Mooring 5 sampled regularly throughout each deployment.

On the fixed-sensor moorings, the only major instrument failure was of an upward-looking ADCP deployed at the bottom of Mooring 4 (mean sensor depth of 3639 m) for the 2004–2006 period. (No usable data were recovered.) The temperature/conductivity sensor at this level functioned normally, as did the VACM mounted above at a mean depth of 3240 m.

2.2. Data processing procedures

Standard data reduction procedures were applied to the Line W shipboard observations. Laboratory sensor calibrations were performed on the CTD sensors prior to or just after each cruise. The water sample salinity and dissolved oxygen data were quality controlled, then used to derive adjustments to the CTD conductivity cell and oxygen sensor data. (See WOCE (1994) Operations Manual Report no. 91-1 for details.) We judge the pressure and temperature data to have uncertainties of 1 dbar and around 0.001 °C, respectively. An estimate of the uncertainty in our shipboard CTD salinity data may be had by deriving the salinity on selected deep isotherms from common sites on all of our cruises for regions and depths where we believe there is little spatial variation or temporal change on multi-year time scale. Such analyses suggest the Line W shipboard CTD salinity data has an uncertainty of 0.002 (standard deviation about the mean salinity on selected deep isotherms from the Sargasso Sea). Much of this variability is due to cruise-to-cruise offsets in the water sample salinities. Applying offsets to the salinity data from selected cruises to improve the consistency of deep water potential temperature–salinity can reduce the salinity scatter by a factor of 2. The processed Line W shipboard data may be downloaded from the project web site: http://www.whoi.edu/science/PO/linew/index.htm or accessed via national data archives.

In similar fashion, the pressure and temperature data from the moored instruments (both profiling and fixed) were processed taking into account laboratory sensor calibrations performed before and/or after each mooring setting. These laboratory data indicate uncertainties of at most 1–2 dbar and 0.001–0.002 °C. Pressure data from the available gauges on Moorings 2 and 4 were used in conjunction with a simple mooring response model to derive pressure time series for each fixed sensor on the moorings not equipped with a pressure sensor.

The raw moored conductivity data from both profiling and fixed instruments exhibited shifts of 0.1 mmho or more during deployments. This behavior appears due chiefly to biological material that on occasion impacted the conductivity cells, as opposed to any growth on the instruments. Most often, the offending material would flush out after a day or two, with the conductivity data returning back towards previous values (but frequently with residual offset). To calibrate the MMP conductivity data from Moorings 3 and 5, a profile-by-profile multiplicative adjustment was derived to achieve (near) constant salinity on selected deep potential isotherms. The process involved working with potential conductivity (conductivity inverted from preliminary salinity and potential temperature referenced to 0 dbar) that, like potential temperature and salinity, is invariant to adiabatic heave. The calibrated ship CTD data were analyzed to estimate potential conductivity on selected potential isotherms that were present on most of the MMP profiles from a deployment. Ratio time series of reference potential conductivity to that from each MMP profile were constructed and used to derive adjusted MMP salinity profiles. Badly fouled segments of conductivity profiles were interpolated using data above and below the offending section as well as profiles acquired before and afterwards in time. The resultant MMP salinity data has minimal potential temperature–salinity variability at depth. For example, the processed 4-year record at Mooring 3 exhibits a minimum-to-maximum range of estimated salinity on the 2.3 °C potential temperature surface (mean depth of 2900 m) of 0.004 with full-record standard deviation of the anomalies from the record mean of 0.0008. (Intrusions and residual errors are responsible for the remaining variability.) At Mooring #1, the water depth precluded MMP sampling to levels where the potential temperature–salinity relationship was tight and invariant. Overall deployment adjustments were derived to bring the data into agreement with available ship data, with profile-specific adjustments applied just to those data that were wildly out of agreement with neighboring profiles. The standard deviation of salinity on the 3.25 °C surface at Mooring 1 (mean depth of 1909 m) is 0.003: a factor of 4 larger than the variability at the bottom of Mooring 3 but likely representing real water mass variability.

Potential temperature–salinity data from the neighboring MMP moorings were used to derive conductivity adjustments for the fixed sensor data from Moorings 2 and 4. The standard deviations of the departure of adjusted salinity data from deployment-mean potential temperature–salinity curves are around 0.003 for deep sensors and increase with height (to, for example, 0.008 at 1000 m on Mooring 2) where natural variability exceeds the sensor uncertainties.

Shipboard LADCP velocity profile data were processed following techniques described by Fischer and Visbeck (1993) and Visbeck (2002). In general, LADCP velocity uncertainties can vary with location, depth and occupation depending on acoustic scatterer density and the performance of the instrumentation. An individual Line W LADCP velocity estimate over the continental slope is believed to have an uncertainty ranging between 2 and 5 cm s^{-1}, with the error thought to be largely independent profile to profile. This uncertainty is comparable to the ageostrophic "noise" signal in the slope waters. Current meter data from the Line W array between 1000 and 3600 m depth indicate that the super-inertial motions (high-pass filtered data with 36-h cutoff period) have rms amplitudes of 2–3 cm s^{-1}.

Matlab-based data reduction tools were used to process the Line W VACM velocity data following procedures developed by the WHOI Buoy Group and refined by R. Beardsley, N. Hogg and B. Owens (personal communications, 2009). Most of the instruments were set up to log vector-averaged velocity estimates at 1/2 h interval. (A few of the meters on MMP moorings logged at 1/4 h interval.) The standard data reduction procedure assigns a speed of 1.3 cm s^{-1} to samples with smaller speed estimates to address rotor stall error, and applies direction estimates based on the recorded compass and vane reading made by the VACM at those times. Fortunately episodes of rotor stall are rare in the Line W data set, occurring less than 4% of the time with each stall event typically lasting less than 1 h. We believe the accepted VACM speed uncertainty of $\sim$1 cm s^{-1} and direction uncertainty ($\sim$3°—comparable to the resolution of the compass measurements: 2.8°) are representative of the Line W data set (McCullough, 1975; Lentz et al., 1995). Magnetic declination estimates were obtained for each mooring deployment from the web site http://www.ngdc.noaa.gov/geomagmodels/Declination.jsp and used to rotate the velocity data to geographic coordinates.

Unlike VACMs, the MMP logs raw sensor data allowing velocity corrections during post processing. MMP velocity profile data in geographic coordinates were derived after applying adjustments to the 3-axis fluxgate compass observations to account for offsets in the three components of logged data as well as orientation of the compass relative to the sting of the acoustic current meter (ACM). Magnetic declinations were applied as above. MMP direction data were further refined using comparisons with simultaneous VACM observations at times when MMPs were within 50 m vertically of the current meters. Some of the early MMP data sets required direction adjustments of 10–20° to achieve consistency: a problem traced to laboratory procedures for estimating the MMP compass orientation in the instrument body. After correction, mean current direction differences between simultaneous VACM and MMP observations were less than 2°. Later MMP deployments returned mean current direction differences with VACM observations that were less than 2° based solely on laboratory compass calibration data. MMP current speed estimates were also compared with VACM observations, after correcting for bias error. The bias adjustments involved estimating for each deployment and applying a depth-varying, time-invariant offset to the raw path speed estimates from the ACM. (These path speed biases of 1–2 cm s^{-1} amplitude varying quasi-sinusoidally on $\sim$500 m wavelength are thought to be caused by impedance variations in the ACM transducer leads with pressure and/or temperature.) Under the assumption that at some point during a year-long deployment, the true ocean current at each depth falls to near zero, the bias profile for each ACM velocity path was taken as the minimum observed speed at each depth during the deployment. After bias correction, average speed differences between VACMs and MMPs at times when the Profilers were within 50 m of the fixed sensor were typically around 1 cm s^{-1} or smaller.

MMP temperature, salinity and velocity data from each profile were gridded to 2 dbar vertical resolution. These final data may be downloaded from the project web site: http://www.whoi.edu/science/PO/linew/index.htm or accessed via national data archives.

2.3. Additional data reduction and analysis procedures

The focus of the present study is the sub-inertial-frequency variability in DWBC transport. Driven by the sampling scheme for the MMPs, the basic data consists of 5-d samples of low-pass-filtered density and velocity observations. The profiles in each burst of MMP sampling were averaged, yielding estimates in which the inertial and semi-diurnal tidal variance is greatly reduced. For consistency, the fixed sensor data were low-pass filtered (36-h filter cutoff period) and subsampled at 5-d interval aligned with the MMP burst times.

Addressing the loss of data from the upward-looking ADCP deployed at 3639 m on Mooring 4 for the 2004–2006 period, for the present analysis, velocity data from the deepest VACM on this mooring at an average depth of 3240 m was extended uniformly to the bottom. Temperature and salinity data from the ADCP level were available throughout the period. A VACM placed at the bottom of Mooring 4 for the 2006–2008 period returned a full record.

As noted earlier, the one major MMP failure in the period was on the 2006–2007 deployment of Mooring 1. Profile data in this gap were synthesized using the observations from the fixed sensors at the top and bottom of this mooring and from the adjacent Mooring 2. A regression procedure was developed to predict anomalies of temperature, salinity and velocity at Mooring 1 from mean profiles based on the 3 years of recovered data from that site. Regression coefficients were determined from the 3 years of complete data and applied to the 2006–2007 period. The resulting synthetic anomaly profiles at 5-d interval were subsequently added to the 3-year-mean profiles to fill the 2006–2007 gap. These same regressions were also applied to times when full profile data from Mooring 1 was available to assess error. Squared correlation between the synthesized and observed observations at Mooring 1 decreased roughly monotonically with height from 1.0 at the bottom (where fixed T/S and current meter data were available) to below 0.5 above 1000 m depth.

At other times and mooring sites, MMP profiles that failed to reach fully between top and bottom stop depths were extrapolated using the fixed sensor data in conjunction with the partial profile observations. For each MMP mooring site, time-mean potential temperature and potential temperature–salinity relationships were derived using all available profile data. Temperature and salinity estimates for short profiles were derived using the mean potential temperature profile (strained to match the observed data at each interpolation time) and the mean potential temperature–salinity relationship. Missing velocity data were estimated by linear interpolation. In most cases, individual short profiles within each MMP burst were extrapolated prior to forming the burst-averages. Observations at burst times when no profile data were available (either due to the MMP being stuck or having exhausted its battery) were synthesized similar to how the 2006–2007 Mooring 1 gap was filled using profile data before and after the vacant burst times and coincident data from fixed sensors on the MMP mooring and the adjacent fixed-sensor moorings.

A final step in the data processing involved construction of temperature, salinity and velocity profiles at 5-d interval for Mooring sites 2 and 4. The T/C sensor and VACM records from each mooring were low-pass filtered and data were extracted at each burst time. These estimates were subsequently spline-interpolated to 2-dbar vertical resolution. The neighboring MMP temperature and salinity profile data at each sample time (shifted vertically to match at observations at the top of the mooring) were then used to extend these synthesized profiles up to 500 dbar. Velocity at the top of each mooring was carried uniformly up through this extrapolation interval. Uniform velocity extrapolation was motivated by empirical orthogonal function analyses of the burst-averaged data from the MMP moorings in which the leading velocity modes (accounting for 60–80% of the velocity anomaly variance) were barotropic in character (single-signed in depth as opposed to all higher modes).

For context, average property sections along Line W were derived from the ship observations. To construct these mean sections, the so-called stream-coordinate averaging was performed. Those stations from each occupation at and south of the Gulf Stream North Wall were shifted laterally to align each synoptic North Wall realization with the mean along-track distance of the front from a reference position at the continental shelf break. The along-track distances for those stations shoreward of the North Wall in each realization were then strained to fit between the shelf break and mean North Wall position. The strained along-track distance for a given Slope station was calculated as the geographic distance of that station from the shelf break multiplied by the ratio of the mean distance of the North Wall to that distance in the respective synoptic section. Each set of stations from a cruise was then mapped onto a common along-track grid prior to isopycnally averaging the ensemble of realizations at each grid site and then remapping into depth space.

2.4. Transport estimation

The focus of the present analysis is DWBC transport in 4 layers bounded by neutral density surfaces (Table 3). The analysis was done in a rotated coordinate system aligned with the mooring line (and roughly orthogonal to the local isobaths). The conventional geographic coordinate axis was rotated 61° clockwise. Thus equatorward across-line velocities and transports are reported as negative values. The available profile estimates from each mooring site were analyzed to first find the depths of the bounding neutral density surfaces and identifying which 2-dbar samples fell within those bounds. Each mooring's contribution to the transport in each layer was calculated by summing the product of these across-line (northeastward–southwestward) velocity estimates, thickness of each 2-dbar cell, and a corresponding width function (which varied with depth). The nominal width function at each site was given by the distances between the midpoints of the adjacent moorings. This distance was truncated on the up-slope side of each mooring at that point where the sloping sea floor intervened. Mooring 5's assigned width extended to the midpoint between Moorings 5 and 6. Time series of layer thickness, average potential temperature and average salinity were also derived. These layer transport time series were subsequently interpolated in time to common, uniform 5-d increment. (This last step was necessitated by the 7.5-d burst interval of the MMPs on Moorings 3 and 5 during the 2005–2006 deployment period.)

For each 5-d time period, the transport streamfunction for each layer was estimated by cumulatively summing the transport estimates from each mooring site (beginning with Mooring 1). The DWBC transport at each time was defined by the southward extremum in the transport streamfunction over the array extent. Transport underestimation error at times when the equatorward DWBC flow broadened beyond the extent of the array is assessed below.

Although not the focus of this study, for completeness and reference to other work, transport estimates were also made for the surface layer (between the free surface and the 27.8 neutral density surface defining the top of the ULSW layer). Guided by the ship observations and analysis of data from Moorings 1 and 3 that suggested the velocity fluctuations were to first order independent of depth, velocity estimates at each mooring site were

Table 3
Layer definitions and bounding neutral density surfaces.

Layer	Neutral density	Average depth (m)
	27.800	678
ULSW		
	27.897	1095
CLSW		
	27.983	1958
ISOW		
	28.066	2771
DSOW		
	28.125	3575

ULSW: Upper Labrador Sea Water; CLSW: Classical Labrador Sea Water; ISOW: Iceland-Scotland Overflow Water; DSOW: Denmark-Strait Overflow Water.

extrapolated up uniformly from the shallowest measurement depth. As this was a 1000 m interval in the case of Moorings 2, 4 and 5, the present surface layer transport estimates are very uncertain. Far more accurate estimates of upper-ocean Slope Water flow may be derived from the *M/V Oleander* ADCP program (see Flagg et al., 2006; http://www.po.gso.uri.edu/rafos/research/ole/index.html).

Shipboard profile data from each cruise were analyzed similarly to estimate DWBC transport in the 4 layers. LADCP velocity profile data, rotated as above, were combined with neutral density profiles based on the ship CTD data and integrated to the southward extremum in the transport streamfunction. In those two cases when the streamfunction extremum was south of Mooring 5, the integration was also estimated over the spatial extent of the moored array (for comparison purposes).

2.5. Supplemental observations

As part of our analysis, we investigated the relationships between DWBC transport and the position of the Gulf Stream and associated Warm Core Rings. For this purpose, we accessed an operational US Naval Oceanographic Office ocean frontal analysis product for our study area that defined the position of the sea surface temperature front marking the North Wall of the Gulf Stream every 2nd day during our study period. A separate data file reported the location and radius of Rings in our region. The intersection latitude of the North Wall and Line W was derived for each frontal map and interpolated onto the 5-d time base of the moored array products. In addition, times when Rings were within 50 km of Line W were recorded.

3. Results

Time-averaged velocity and water property sections based on the ship data provides context for the analysis of the moored array data (Fig. 2). The Gulf Stream at Line W on average extends over the full depth with a characteristic tilt of the zero velocity contour that extends offshore with increasing depth. The core speed that approaches 2 m s^{-1} at the surface decays to less than 0.5 m s^{-1} below 500 m. The DWBC lies shoreward of the Stream over the continental slope. Typical mean DWBC speeds are around 5 cm s^{-1}, with comparatively little variation in depth. Consistent with this, mean isopycnals tend to be rather flat in the DWBC whereas they slope steeply in the Gulf Stream reflecting the thermal wind balance. On average at Line W (and elsewhere between Cape Hatteras and Grand Banks), the poleward and equatorward limbs of the Atlantic MOC lie side by side rather than one atop the other.

3.1. Time-averaged transport

The Eulerian-mean data from the moored array provide a similar picture to the ship data, albeit with more limited lateral and vertical extent (Fig. 3). Owing to the vastly greater number of independent realizations of the velocity field provided by the moored array than were obtained by ship survey, subtle spatial structure in the mean velocity distribution is evident. In particular, a mid-depth equatorward velocity extremum is observed about Mooring 1 with bottom-enhanced equatorward flow at Moorings 2 and 4. (We do not believe the differences in these average velocity depictions are due to averaging procedures as the station distance straining used to derive Fig. 2 introduced only small horizontal displacements of the slope stations. Effectively Fig. 2 represents an Eulerian mean of the ship stations over the slope.) One might question if this latter pattern of mean meridional flow is an artifact of the different sensors employed on the moorings, but this spatial structure in the mean velocity is replicated by the bottom VACMs on each of the moorings (common instrument type and sampling characteristics).

Meridional transports in the water mass layers were estimated using the Eulerian-mean velocity field of Fig. 3 (Table 4). Recognizing that such transport estimates can be biased in the case of a meandering jet, mean transport estimates were also derived from the 5-d-resolution moored array data as described in Section 2.4. (For the remainder of this paper, we focus principally on the latter transport estimates.) For the sum of the 4 water mass layers, we estimate a mean meridional transport of -25.1×10^6 m^3 s^{-1} (negative value denotes equatorward flow). Lagged autocorrelation function analysis was performed on the transport time series of each water mass layer and of the 4-layer summed transport series. Decorrelation time scale estimates for these series (defined as twice the integral of the normalized lagged autocorrelation functions to their first zero crossings) ranged from 18 days for the ULSW layer to 10 days for the DSOW layer, and 16 days for the time series of the 4-layer sum. Based on the latter and associated standard deviation reported in Table 4, we estimate statistical 95% confidence bounds on the 4-layer-summed mean transport of $\pm2.7\times10^6$ m^3 s^{-1}. Our mean transport estimate for the 5-layer-summed transport (previous 4-layer sum plus the estimated surface layer transport) is $-32.5\pm3.4\times10^6$ m^3 s^{-1} (where the uncertainty only encompasses the effects of temporal variability, not error in vertical extrapolation). For comparison purposes, a uniform 1 cm s^{-1} velocity bias applied to the estimated mean area of the 4-layer-summed DWBC results in a transport error of 5.8×10^6 m^3 s^{-1}. While 1 cm s^{-1} is the estimated uncertainty in the individual velocity estimates from the array, there is no reason to believe the errors of all the current meters in the array are correlated. We believe that statistical uncertainty deriving from temporal variability and bias due to the finite extent of the array (see below) dominate the error in our mean array transport estimates.

One concern with the finite-extent of the Line W moored array is that it may at times miss some transport associated with equatorward flow lying south of Mooring 5. For the ULSW layer in the 10 May 2004–9 April 2008 period, the point along the array where the cumulative equatorward transport extremum was located (effectively a zero crossing of the meridional velocity with distance offshore) was clearly within the spatial extent of the array 66% of the time. That is, the ULSW transport extremum occurred north of Mooring 5 66% of the time. This analysis may be extended using the US Navy frontal analysis product. Based on those data, we estimate that the North Wall of the Gulf Stream was north of the midpoint between Moorings 5 and 6 (and thus the ULSW equatorward transport was fully captured by the array) 80% of the present analysis period. Those times when the Stream was displaced well south and some transport may have been missed typically occurred in spring with each continuous episode of southward displacement beyond the array lasting 1–2 weeks. Importantly, during those times, the average North Wall position was south of the Mooring 5–6 midpoint by only 25 km. Based on an average ULSW layer thickness of 357 m at Mooring 5 and mean equatorward velocity of the ULSW layer of 5 cm s^{-1}, the array missed on average only 0.5×10^6 m^3 s^{-1} of equatorward ULSW transport during times when the Gulf Stream meandered south of the array. This translates to a 2% underestimation of the Stream-coordinate Mean ULSW transport estimate reported in Table 4. The Bias-adjusted mean transport estimate is also given in Table 4.

Owing to the mean slope in the boundary between the DWBC and deep Gulf Stream (zero velocity contour is located increasingly offshore with depth, see Fig. 2), it is likely that larger

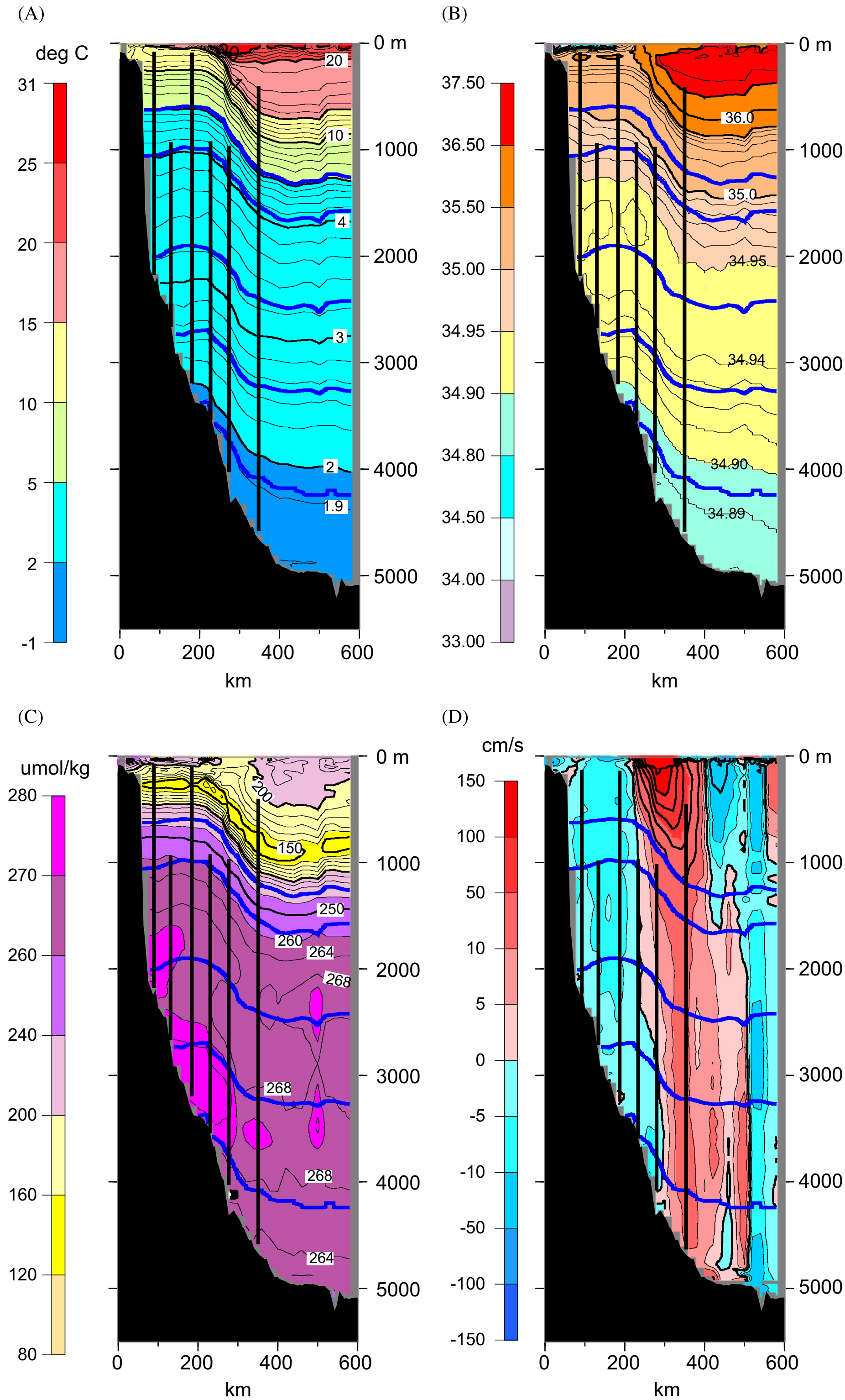

Fig. 2. Line W stream-coordinate-averaged depth-distance sections (see Section 2.3) of (A) potential temperature, (B) salinity, (C) dissolved oxygen and (D) across-line velocity based on ship observations. Negative velocities correspond to southwestward flow. Also shown on each panel are the positions of the Line W moorings and the 5 neutral density surfaces taken to define the water mass layers of the DWBC.

fractions of equatorward transport in the denser water mass layers were missed by the array. To assess these errors, we analyzed the deepest VACM records from Moorings 5 and 6 for the common period of deployment (24 August 2005–1 October 2007) assuming the instrument on Mooring 6 functioned normally after the top of the mooring fell to the bottom. The common-period-mean across-line velocity at the deepest VACMs on the two moorings were similar ($-4.1\ \mathrm{cm\,s^{-1}}$ at Mooring 5, $-2.7\ \mathrm{cm\,s^{-1}}$ at Mooring #6) and the variations in low-passed across-line velocity anomalies at the two sites (filter cutoff period

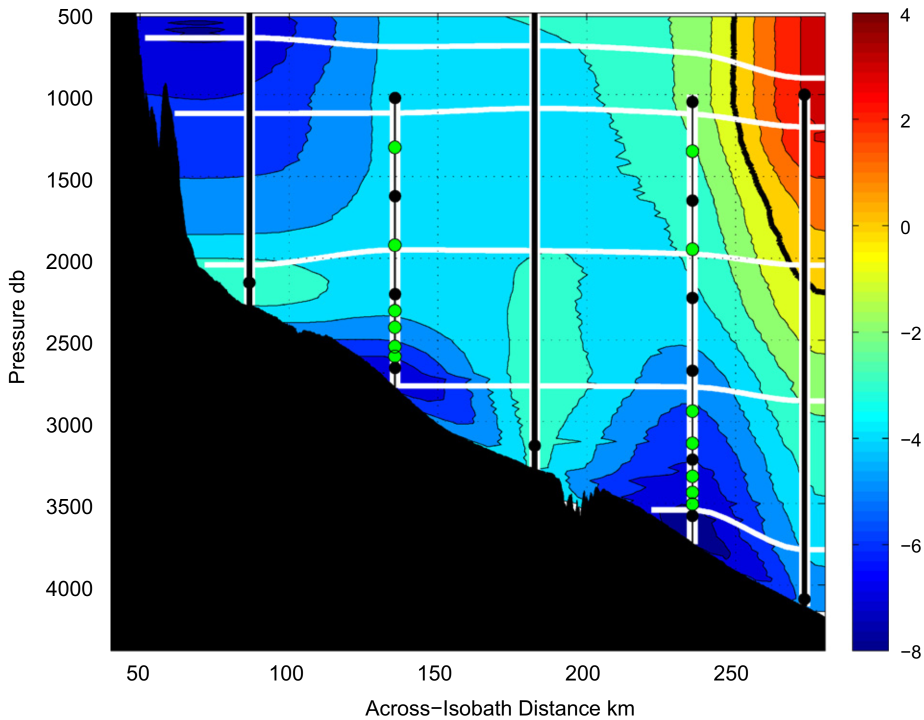

Fig. 3. Eulerian-mean across-line velocity distribution based on the 2004–2008 Line W moored array data. The contour interval is 1 cm s^{-1}; the thick black contour marks the 0 isotach. Also shown are the position of the 5 primary moorings with sensor depths indicated, and mean locations of the 5 neutral density surfaces used to partition the DWBC waters. Negative velocities correspond to southwestward flow normal to the array. Current meters are marked with black dots while T/C recorders are indicated with green dots. The thick black lines mark the depth intervals sampled by MMPs.

Table 4
Mean meridional (cross-line) transport estimates and variability for the period 10 May 2004 to 9 April 2008. See Table 3 for layer definitions. The surface layer extends from the surface to the 27.8 neutral density surface. Since significant vertical extrapolation was required for this layer, the reported transport estimates are uncertain. The 4-layer Sum is for the ULSW, CLSW, ISOW and DSOW layers; the 5-layer Sum includes the surface layer. Bias-adjusted mean transport estimates as described in the text are also given.

Layer	Stream-coordinate Mean 10^6 m^3 s^{-1}	Bias Adjusted 10^6 m^3 s^{-1}	Standard Deviation 10^6 m^3 s^{-1}	Eulerian Mean 10^6 m^3 s^{-1}
surface	−7.4	−7.5	4.5	−4.7
ULSW	−4.8	−4.9	2.3	−3.6
CLSW	−8.4	−9.2	4.2	−5.9
ISOW	−6.4	−7.6	3.7	−4.5
DSOW	−5.5	−7.0	3.9	−4.0
4-layer Sum	−25.1	−28.7	12.5	−18.0
5-layer Sum	−32.5	−36.2	15.9	−22.7

of 36 hours) were significantly correlated at the 95% confidence level. (Maximum correlation was 0.25 at a lag of 11 days; Mooring 5 led 6 which is typical of Topographic Rossby Wave motions at this site, see Fratantoni and Pickart (2003). Examining the full 5-element-array estimates of DSOW transport during the common deployment period, we estimate that one-third of the time, deep flow about Mooring 6 would have added to the estimated equatorward transport in the DSOW layer. (These were times when the DSOW transport streamfunction based on the 5 main Line W moorings achieved its maximum equatorward value at Mooring 5 and the bottom VACM on Mooring 6 recorded southward flow.) The mean meridional velocities at the two mooring sites at these times were similar (-11.7 cm s^{-1} at #5 vs. -9.5 cm s^{-1} at 6). If we assume an additional DSOW transport contribution from Mooring 6 equal to the mean Mooring 5 contribution at these times of extreme southward Gulf Stream displacements (-4.5×10^6 m^3 s^{-1}), we arrive at a Bias-adjusted mean DSOW transport of -7×10^6 m^3 s^{-1}. This suggests the Stream-coordinate Mean DSOW transport reported in Table 4 is underestimated by 1.5×10^6 m^3 s^{-1} (27%). Bias adjusted mean transports for the surface, CLSW and DSOW layers reported in Table 4 were derived by linear interpolation.

3.2. *Transport variability*

The 5-d, 4-layer-summed meridional transport estimates in the 10 May 2004–9 April 2008 period ranged between -3.5 and -79.9×10^6 m^3 s^{-1} (Fig. 4). Reasonable, but by no means perfect agreement is seen between the synoptic transport estimates from the moored array and the shipboard measurements. For the 4-layer summed transports, the difference between the 7 ship-based transport estimates (those acquired while the array was fully operational, with integrations limited to the horizontal extent of the array) and the synoptic array estimates (interpolated to the mean time that each of the ship sections were occupied) range between -4 and $+19\times10^6$ m^3 s^{-1} with a mean of 8×10^6 m^3 s^{-1} and standard deviation of 7×10^6 m^3 s^{-1}. (These reported differences are of the ship transport estimates minus those from the array.) These differences are small in comparison to the range in transport estimates derived from the array and arguably consistent with the uncertainty in individual shipboard transport estimates.

On two occasions (April–May, 2005; September, 2007), the latitude of the transport streamfunction extremum for the water mass layers based on the shipboard data was beyond the meridional extent of the 5-element moored array. In the first case, an additional -53.4×10^6 m^3 s^{-1} of meridional transport

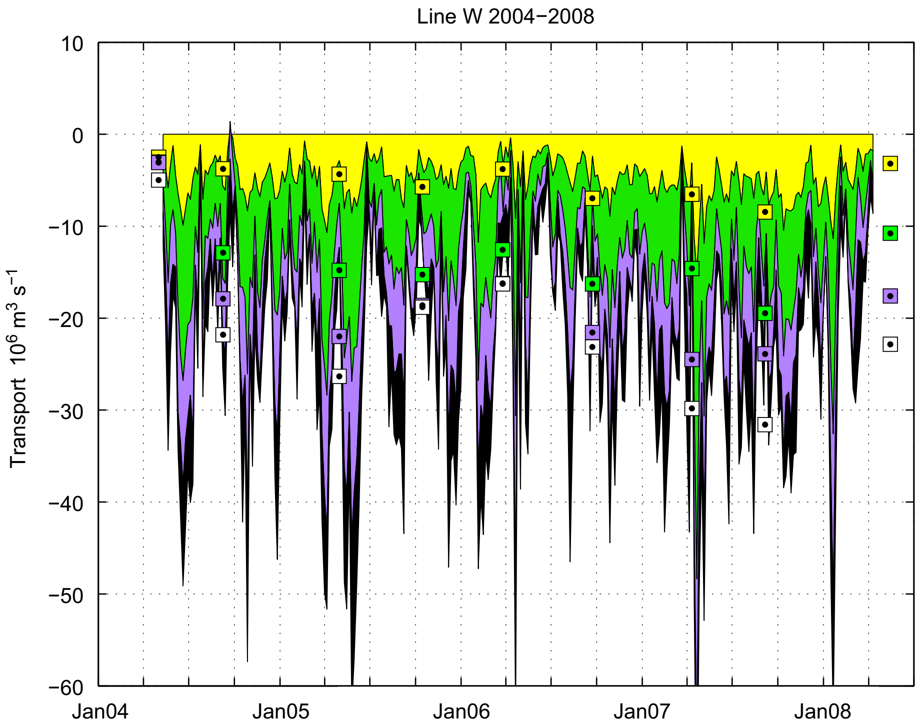

Fig. 4. Time series of meridional DWBC transport partitioned by layer for the period 10 May 2004 to 9 April 2008. Negative values correspond to equatorward flow. The colors denote: ULSW-yellow, CLSW-green, ISOW-purple, DSOW-black. Squares indicate the corresponding transport estimates based on cruise observations limited to the extent of the moored array.

(contributions from all four layers) was measured from the ship. The other occasion had only $-4.3\times10^6\ \mathrm{m^3\,s^{-1}}$ of additional meridional transport limited to the ISOW and DSOW layers. The April–May 2005 cruise took place during an extreme southward meander of the Gulf Stream at Line W when the North Wall along Line W was at 37°N. The Navy frontal analysis product slightly underestimates the southward frontal excursion at this time, but does indicate it was a local period of significant southward displacement. Comparable equatorward excursions at other times are rare in the North Wall position record (4 episodes, each lasting only a few days).

No obvious relationship was found between DWBC transport and proximity of Warm Core Rings to the array. However, a statistically significant correlation was observed between boundary current transport and meridional position of the Gulf Stream, of the sense that stronger equatorward DWBC transport corresponded to southward displacements of the Gulf Stream (Fig. 5). A correlation of 0.38 is obtained between the 5-d 4-layer-summed transport estimates and local intersection latitude of the North Wall and Line W. This increases to 0.55 for low-pass-filtered time series (cutoff period of 50 days), perhaps as one of our reviewer suggests, due to the removal of Topographic Rossby Wave variability. Using the longer decorrelation time scale of 23 days for the North Wall latitude, the 0.38 correlation is significantly different from zero at the 95% confidence level (as is the correlation between the low-pass-filtered series using a 50-d decorrelation time scale).

Decomposing layer area variability, layer thickness variations were found to be of secondary importance to layer width fluctuations. Visually, the dominant correlated low-frequency signal in DWBC transport and Gulf Stream position appears seasonal with a tendency for greater transport and southward Stream displacement in spring. Obviously with just a 4-year-long record, we can make no statistically significant statements about the mean seasonal cycle. Based on satellite altimeter data for the period 1992–2008, Peña-Molino and Joyce (2008) and Peña-Molino (2010) derived a mean seasonal cycle for Gulf Stream axis position that had maximum southward displacement in spring. However, a 2-sample F test for equal variances indicates that this annual cycle accounts for no significant variance in the record of Gulf Stream position at the 0.05 significance level.

Although the transport variations we observe are correlated with the Gulf Stream position, and hence, with the area experiencing equatorward flow over the continental slope, the transport variations are more than kinematic. Based solely on the array data, we obtain a correlation of -0.64 between 4-layer DWBC transport fluctuations (T) and area of equatorward meridional flow (A; larger area corresponding to greater equatorward transport), but a larger correlation of 0.78 between transport and average DWBC velocity (v; time series constructed by dividing the 4-layer DWBC transport estimates by the corresponding DWBC area estimates). Both correlations are significantly different from zero at the 95% confidence interval based on an estimated 16-d decorrelation time scale. Decomposing the 4-layer DWBC transport estimates into time mean and fluctuating components of the 4-layer area and spatially averaged velocity ($T=vA=v'\overline{A}+\overline{v}A'+v'A'$) we find that fluctuations in DWBC velocity contribute approximately twice as much to the total 4-layer transport variance as do DWBC area fluctuations. Specifically, the variance of the series $v'\overline{A}$ contributes about 60% the variance of the full 4-layer transport anomaly record, while that for the product $\overline{v}A'$ contributes about 30% to the total transport variance. The cross product term ($v'A'$) accounts for the remaining variance.

4. Discussion

We find statistically significant correlation between Gulf Stream position and DWBC transport. Our 4-year-long record is only able

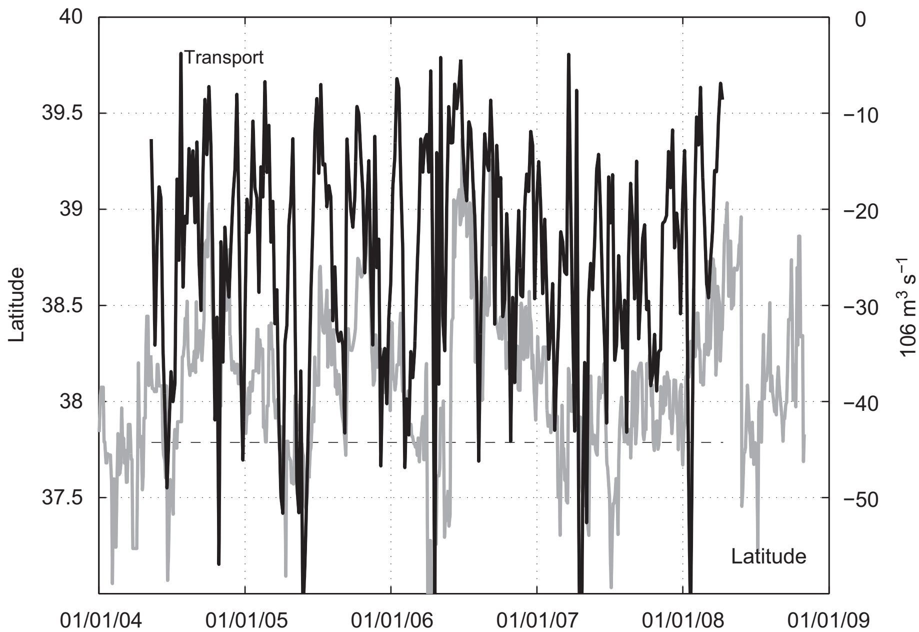

Fig. 5. Time series of Gulf Stream North Wall latitude at Line W (gray curve) and 4-Layer Sum meridional transport (sum of ULSW, CLSW, ISOW and DSOW layer transports; negative indicates equatorward flow). The dashed line marks the southern extent of the 5-element moored array; DWBC transport estimates at times when the North Wall was south of the array are underestimated.

to shed light on seasonal and shorter period variations. For longer time scales, Rossby and Benway (2000) and Peña-Molino and Joyce (2008) report correlations between Gulf Stream position and Slope Water temperatures (southward displacements associated with colder Slope Waters) and suggested possible causal mechanisms in which the DWBC influences the path of the Stream. We do not know if similar mechanisms are operating on the shorter time scales resolved by the Line W program but are actively investigating the question.

The short duration of the moored record raises questions about the representativeness of the present results to the long-term mean. While estimates of intermediate and deep water transport at Line W are limited to the present 2004–2008 period, remote sensing products span a much longer time interval. Peña-Molino Peña (2010) used satellite altimeter data to estimate a time series of Gulf Stream axis latitude on Line W for the period 29 September 1992–28 April 2008. Based on these data, the satellite-record-mean axis latitude is indistinguishable at the 95% confidence level from the average latitude for the Line W moored array deployment period discussed here. Assuming the relationship between Gulf Stream position and DWBC transport documented by the Line W moored measurements holds, this result suggests that the estimates reported in Table 4 are representative of the much longer altimeter satellite era.

Estimates of water mass formation rates by LeBel et al. (2008) provide context to the present DWBC transport estimates. These investigators deduced formation rates from changes in North Atlantic tracer inventories for a series of layers bounded by the same, or nearly same neutral density surfaces as used here. LeBel et al. (2008) report average formation rates for the period 1970 to 1997 of ULSW: $3.5\times10^6\,m^3\,s^{-1}$; CLSW: $8.2\times10^6\,m^3\,s^{-1}$; ISOW: $5.7\times10^6\,m^3\,s^{-1}$; DSOW: $2.2\times10^6\,m^3\,s^{-1}$, with uncertainties of $\pm20\%$ for the CSLW layer and $\pm16\%$ for the overflow layers. While these formation rates are remarkably similar to the Line W time-averaged DWBC transport estimates in Table 4, why that is the case is not obvious given the possible contributions to net meridional transport at the Line W latitude from recirculations and interior meridional flows not represented in our boundary current transport figures.

The present mean DWBC transport estimates are perhaps more straightforwardly comparable to transport estimates reported by Johns et al. (1995) based on moored observations about 68°W. The Johns et al. analysis combined data from the SYNOP array (deployed from June 1988 to August 1990) that was located about the mean axis of the Gulf Stream (moorings at and deeper than the 3500 m isobath) with earlier moored data from the RISE and SEEP experiments over the continental slope to synthesize a map of the mean equatorward flow in the DWBC (see their Fig. 14). Stream-coordinate averaging was performed on the SYNOP data; Eulerian mean velocities were taken over the slope. Based on their derived time-averaged velocity section, Johns et al. report a time-mean, total meridional transport north of the Gulf Stream of $-40\pm10\times10^6\,m^3\,s^{-1}$. While our best estimate of mean total meridional transport in Table 4 ($-36.2\times10^6\,m^3\,s^{-1}$) is a bit less than this, we note that the present estimates do not include the flow of waters denser than neutral density 28.125. Even without factoring this missing transport, the uncertainties of the two estimates overlap. Thus we conclude that there has been no detectable change (difference greater than the admittedly large measurement uncertainties) in multi-year-averaged equatorward DWBC transport about 70°W between 1988–1990 and 2004–2008.

This conclusion is reminiscent of the statement by Schott et al. (2006) who analyzed moored array data obtained east of Grand Banks and compared data from 1993 to 1995 with observations from 1999 to 2005. Over this time interval, Schott et al. found no significant change in equatorward DWBC currents. Time-averaged transport estimates from these arrays about 42°N provide another interesting point of comparison with the present Line W estimates. Partitioning the water column into water mass layers defined by potential density surfaces that align closely with the neutral density layer partitions used here, Schott et al. (2004) estimated the following Eulerian-mean meridional transports—ULSW: $-0.7\times10^6\,m^3\,s^{-1}$; CLSW: $-3.3\times10^6\,m^3\,s^{-1}$; ISOW (termed Northeast Atlantic Deep Water by Schott et al.): $-4.3\times10^6\,m^3\,s^{-1}$; DSOW: $-4.6\times10^6\,m^3\,s^{-1}$. That this level of agreement is found with the Eulerian-mean transport estimates shown in Table 4 is surprising given the different regional circulations that exist about these two arrays. Indeed, significantly greater DWBC transport was anticipated at Line W compared to Grand Banks due to the Northern Recirculation Gyre (e.g., Hogg et al., 1986; Hogg, 1992; Johns et al., 1995). Evidently much of the Recirculation Gyre contribution to equatorward flow in the Slope Sea must be entrained by the Gulf Stream and returned back northwards prior to reaching Line W.

Sensible transport comparisons with the observations from 26°N being made by the UK–US RAPID/MOCHA programs (e.g., Cunningham et al., 2007) are not yet possible. Putting aside the significant intensity differences in the respective local deep water recirculation gyres, the 26°N investigators have to date only reported transports that have been partitioned by depth. The ocean stratification varies markedly between 39° and 26°N; transport comparisons at common depths make no physical sense. Given the relatively flat density surfaces in the interior of the deep Atlantic along 26°N and reasonably tight potential temperature–salinity relationship, it should be possible to derive mean meridional transport estimates in density classes from the RAPID/MOCHA data to allow comparison with Line W and observational programs farther north.

Of course a major success of RAPID/MOCHA program is the estimation of net (basin-wide-integrated) meridional transport. The Line W program by itself clearly does not do this. We only occasionally (during our cruises) sample the poleward directed Gulf Stream flows that return northward some of the equatorward flow sampled by our moored array, and have no regular sampling program in the deep interior or eastern basin. We are therefore investigating schemes to combine Line W measurements with satellite altimeter and interior water column observations from profiling floats and other sources (similar to Willis, 2010) to synthesize basin-wide realizations of the stratification and circulation that may be used to derive net meridional transport estimates. In parallel, we are exploring ways to include Line W measurements in North Atlantic state estimation models as an alternate way to document the net Atlantic MOC at 30–40°N as well as to better place the Line W observations in the context of the regional circulation.

Acknowledgments

The observations presented here derive from the efforts, both at sea and ashore, of a large number of talented individuals. We thank them as a group for their dedication and continuing support. One of these technicians, Ryan Schrawder, tragically passed away shortly after the first Line W array deployment cruise. This paper is dedicated to his memory.

Initial observations at Station W (2001–2004) were made possible by a grant from the G. Unger Vetlesen Foundation and support from the Woods Hole Oceanographic Institution. Since 2004, the Line W program has been supported by the US National Science Foundation with supplemental contribution from WHOI's Ocean and Climate Change Institute. Any opinions, findings, and conclusions or recommendations expressed in this publication are those of the authors and do not necessarily reflect the views of the National Science Foundation.

References

Berloff, P., Meacham, S.P., 1998a. The dynamics of a simple baroclinic model of the wind-driven circulation. Journal of Physical Oceanography 28, 361–388.

Berloff, P., Meacham, S.P., 1998b. On the stability of the wind-driven circulation. Journal of Marine Research 56, 937–993.

Berloff, P.S., McWilliams, J.C., 1999a. Large-scale, low-frequency variability in wind-driven ocean gyres. Journal of Physical Oceanography 29, 1925–1949.

Berloff, P.S., McWilliams, J.C., 1999b. Quasigeostrophic dynamics of the Western Boundary Current. Journal of Physical Oceanography 29, 2607–2634.

Bower, A.S., Lozier, M.S., Gary, S.F., Böning, C., 2009. Interior pathways of the Atlantic Meridional overturning circulation. Nature, 243–248. doi:10.1038/nature07979.

Cayan, D.R., 1992a. Latent and sensible heat flux anomalies over the Northern Oceans: the connection to monthly atmospheric circulation. Journal of Climate 3, 354–369.

Cayan, D.R., 1992b. Latent and sensible heat flux anomalies over the Northern Oceans: driving the sea surface temperature. Journal of Physical Oceanography 22, 859–881.

Cunningham, S.A., Kanzow, T., Rayner, D., Baringer M.O., Johns, J., Marotzke, W.E., Ongworth, H.R., Grant, E.M., Hirschi, J.J.-M., Beal, L.M., Meinen, C.S., Bryden, H.L., 2007. Temporal variability of the Atlantic Meridional Overturning circulation at 26.5°N. Science 317, 935–938, 17 August [doi: 10.1126/science.1141304].

Curry, Ruth G., McCartney, Michael S., 2001. Ocean gyre circulation changes associated with the North Atlantic oscillation. Journal of Physical Oceanography 31 (12), 3374–3400.

Curry, R., Mauritzen, C., 2005. Dilution of the northern North Atlantic in recent decades. Science 308, 1772–1774.

Csanady, G.T., Hamilton, P., 1988. Circulation of slopewater. Continental Shelf Research 8 (5–7), 565–624.

Deser, C., Blackmon, M.L., 1993. Surface climate variations over the North Atlantic Ocean during winter: 1900–1989. Journal of Climate 6, 1743–1753.

Dickson, R.R., Lazier, J., Meincke, J., Rhines, P., Swift, J., 1996. Long-term coordinated changes in the convective activity of the North Atlantic. Progress in Oceanography 38, 241–295.

Dickson, R.R., Osborn, T.J., Hurrell, J.W., Meincke, J., Blindheim, J., Adlandsvik, B., Vigne, T., Alekseev, G., Maslowski, W., 2000. The Arctic Ocean response to the North Atlantic Oscillation. Journal of Climate 13, 2671–2696.

Dickson, R., Yashayaev, I., Meincke, J., Turrell, W., Dye, S., Holfort, J., 2002. Rapid freshening of the deep North Atlantic Ocean over the past four decades. Nature 416, 832–837.

Fischer, J., Visbeck, M., 1993. Deep velocity profiling with self contained ADCPs. Journal of Atmospheric and Oceanic Technology 10, 764–773.

Flagg, C.N., Dunn, M., Wang, D.P., Rossby, H.T., Benway, R.L., 2006. A study of the currents of the outer shelf and upper slope from a decade of shipboard ADCP observations in the Middle Atlantic Bight. Journal of Geophysical Research 111, C06003. doi:10.1029/2005JC003116.

Fratantoni, P.S., Pickart, R.S., 2003. Variability of the shelfbreak jet in the Middle Atlantic Bight: internally or externally forced? Journal of Geophysical Research 108, 3166. doi:10.1029/2002JC001326.

Greatbatch, R.J., Fanning, A.F., Goulding, A.G., Levitus, S., 1991. A diagnosis of interpentadal circulation changes in the North Atlantic. Journal of Geophysical Research 96, 22,009–22,023.

Häkkinen, S., Rhines, P.B., 2004. Decline of subpolar North Atlantic circulation during the 1990s. Science 304, 555–559.

Hogg, N.G., Pickart, R.S., Hendry, R.M., Smethie Jr., W.J., 1986. The northern recirculation gyre of the Gulf Stream. Deep-Sea Research A33, 1139–1165.

Hogg, N.G., 1992. On the transport of the Gulf Stream between Cape Hatteras and the Grand Banks. Dee-Sea Research 29, 1231–1246.

Hurrell, J.W., 1996. Influence of variations in extratropical wintertime teleconnections on Northern Hemisphere temperature. Geophysical Research Letters 23, 665–668.

Hurrell, J.W., van Loon, H., 1997. Influence of variations in extratropical wintertime teleconnections on Northern Hemisphere temperature. Climatic Change 36, 301–326.

Johns, W.E., Shay, T.J., Bane, J.M., Watts, D.R., 1995. Gulf Stream structure, transport, and recirculation near 68°W. Journal of Geophysical Research 100, 817–838.

Joyce, T.M., Deser, C., Spall, M.A., 2000. On the relation between decadal variability of Subtropical Mode Water and the North Atlantic Oscillation. Journal of Climate 13 2550–2569.

Joyce, T.M., Dunworth-Baker, J., Pickart, R., Torres, D., Waterman, S., 2005. On the deep Western Boundary Current south of Woods Hole. Deep-Sea Research II 52, 615–625.

Kushnir, U., 1994. Interdecadal variations in North Atlantic Sea surface temperature and associated atmospheric conditions. Journal of Climate 7, 141–157.

LeBel, D.A., Smethie Jr., W.M., Rhein, M., Kieke, D., Fine, R.A., Bullister, J.L., Min, D.-H., Roether, W., Weiss, R.F., Andrie, C., Smythe-Wright, D., Jones, P., 2008. The formation rate of North Atlantic Deep Water and Eighteen Degree Water calculated from CFC-11 inventories observed during WOCE. Deep-Sea Research I 55, 891–910. doi:10.1016/j.dsr.2008.03.009.

Lazier, J.R.N., 1995. The Salinity Decrease in the Labrador Sea Over the Past Thirty Years. Climate on Decade-to-Century Time Scales. National Academy of Sciences Press, Washington, DC, pp. 295–302.

Lentz, L.J., Butman, B., Williams III, A.J., 1995. Comparison of BASS and VACM current measurements during STRESS. Journal of Atmospheric and Oceanic Technology 12, 1328–1337.

McCullough, J.R., 1975. Vector Averaging Current. Meter speed calibration and recording technique. W.H.O.I. Technical Report, Ref. no. 75-44, unpublished.

Peña-Molino, Beatriz, Joyce, Terrence, 2008. Variability in the Slope Water and its relation to the Gulf Stream path. Geophysical Research Letters 35 (LO3), 606. doi:10.1029/2007GL032183.

Peña-Molino, Beatriz, 2010. Variability in the North Atlantic's Deep Western Boundary Current: upstream causes and downstream effects. Ph.D. Dissertation, MIT/WHOI Joint Program, no. 2010–17, 174 pp.

Rogers, J.C., 1990. Patterns of low-frequency monthly sea level pressure variability (1899–1986) and associated wave cyclone frequencies. Journal of Climate 3, 1364–1379.

Rossby, T., Benway, R.L., 2000. Slow variations in mean path of the Gulf Stream east of Cape Hatteras. Geophysical Research Letters 27, 117–120.

Schott, F., Zantopp, R., Stramma, L., Gengler, M., Fischer, J., Wibaux, M., 2004. Circulation and Deep Water export at the western exit of the subpolar North Atlantic. Journal of Physical Oceanography 34, 817–843.

Schott, F.A., Fischer, J., Dengler, M., Zantopp, R., 2006. Variability of the Deep Western Boundary Current east of the Grand Banks. Geophysical Research Letters 33, L21S07. doi:10.1029/2006GL026563.

Silverthorne, K.E., Toole, J.M., 2008. Seasonal kinetic energy variability of near-inertial motions. Journal of Physical Oceanography, doi: 10.1175, JPO3920.

Spall, M.A., 1996. Dynamics of the Gulf Stream/Deep Western Boundary crossover. Part II: low frequency internal oscillations. Journal of Physical Oceanography 26, 2169–2182.

Stommel, H., 1965. The Gulf Stream: A Physical and Dynamical Description, 2nd ed. University of California Press, Berkeley, 248 pp.

Talley, L.D., 1996. North Atlantic circulation and variability. Reviewed for the CNLS conference. Physica D 98 (2), 625–646.

Visbeck, M.H., Cullen, G., Krahmann, Naik, N., 1998. An ocean model's response to North Atlantic Oscillation-like wind forcing. Geophysical Research Letters 25, 4521–4524.

Visbeck, M., 2002. Deep velocity profiling using lowered Acoustic Doppler Current Profiler: bottom track and inverse solutions. Journal of Atmospheric and Oceanic Technology 19, 794–807.

Willis, J.K., 2010. Can In-Situ Floats and Satellite Altimeters Detect Changes in Atlantic Ocean Overturning? Geophysical Research Letters 37, L06602. doi:10.1029/2010GL042372.

WOCE, 1994. Operations Manual, Volume 3: The Observational Programme, Section 3.1: WOCE Hydrographic Programme, Part 3.1.3: WHP Operations and Methods. WHP Office Report WHPO 91-1, WOCE Report No. 68/91, November Revision 1, Woods Hole, MA, USA. Available from 〈http://whpo.ucsd.edu/manuals.html〉.

Yang, J., Joyce, T.M., 2003. How do high-latitude North Atlantic climate signals negotiate the crossover boundary between the Deep-Western Boundary Current and the Gulf Stream. Geophysical Research Letters 30 (2), 1070. doi:10.1029/2002GLO15366.